Constraining $A \to ZH$ with $H \to t\bar{t}$ in the Low-Mass Region

Saiyad Ashanujjaman[©],^{1,2,*} Guglielmo Coloretti[©],^{3,†} Andreas Crivellin [©],^{3,‡} Siddharth P. Maharathy[©],^{4,5,§} and Bruce Mellado[©],^{4,¶}

¹Institut für Theoretische Teilchenphysik, Karlsruhe Institute of Technology, Engesserstraße 7, D-76128 Karlsruhe, Germany

²Institut für Astroteilchenphysik, Karlsruhe Institute of Technology,

Hermann-von-Helmholtz-Platz 1, D-76344 Eggenstein-Leopoldshafen, Germany

³Physik-Institut, Universität Zürich, Winterthurerstrasse 190, CH-8057 Zürich, Switzerland

⁴School of Physics and Institute for Collider Particle Physics,

University of the Witwatersrand, Johannesburg, Wits 2050, South Africa

⁵Indian Institute of Science Education and Research Pune, Dr. Homi Bhabha Road, Pune 411008, India

⁶Institute of High Energy Physics, 19B, Yuquan Road, Shijing District, 100049, Beijing, China.

The decay $A \to ZH$ is a characteristic signal of two-Higgs-doublet models (2HDMs), where A and H lie primarily within the same $SU(2)_L$ multiplet, leading to a coupling of order g_2 to the Z boson. The subsequent decay $H \to tt^{(*)}$ is particularly promising, as it gives rise to distinct final states involving multiple leptons and b-jets. The required splitting between m_A and m_H can naturally occur near the electroweak scale while being consistent with perturbative unitarity. Whereas dedicated ATLAS and CMS searches focused on the region with both top-quarks on-shell, we cover lower masses where one top quark is off-shell by recasting Standard Model $t\bar{t}Z$ measurements of ATLAS and CMS. The obtained limits on $\sigma(A \to ZH) \times \text{Br}(H \to t\bar{t})$ are between 0.12 pb and 0.62 pb. When interpreted within the type-I 2HDM, a sizable part of the so far unconstrained low-mass region is excluded. Interestingly, we observe these stringent limits despite a preference (up to 2.5 σ) for a non-zero new physics signal, most pronounced around for $m_A \approx 450$ –460 GeV and $m_H \approx 290$ GeV, with a best-fit value of $\sigma(A \to ZH) \times \text{Br}(H \to t\bar{t}) \approx 0.3$ pb. This cross section can be accommodated within a top-philic 2HDM for a top-Yukawa coupling of the second Higgs doublet of $\mu_t \gtrsim 0.16$.

I. INTRODUCTION

With the observation of the Brout-Englert-Higgs boson [1–4] at the LHC [5, 6], the particle content of the Standard Model (SM) has been confirmed. While the measured properties of this 125 GeV scalar boson are consistent with SM predictions [7, 8], the existence of additional Higgs bosons is not excluded, provided their contribution in electroweak symmetry breaking is subdominant and their mixing with the SM Higgs is small. In fact, numerous extensions of the SM Higgs sector have been proposed, including $SU(2)_L$ singlets [9–11], doublets [12–18], triplets [19–29], and even higher representations.

The search for new Higgs bosons is a primary goal of the LHC program. Of particular interest are the cascade decays of heavy Higgs states (see Refs. [30, 31] for an overview), such as the decay of a pseudoscalar Higgs boson A into a Z boson and a new scalar H ($A \rightarrow ZH$). Notably, this chain decay has been identified as a 'smoking gun' signature for a strong first-order electroweak phase transition, which could explain the origin of the matterantimatter asymmetry in the Universe [32]. Furthermore, owing to their clean experimental signatures, these processes provide powerful probes of extended Higgs sectors.

In particular, the decay $H \to t\bar{t}$ yields distinctive multilepton final states with *b*-jets, and has been searched for above the top threshold by ATLAS [33] and CMS [34].¹

However, the low-mass region below the top threshold, where one of the top quarks is off-shell, remains essentially unexplored. In this Letter, we close this gap by investigating the process $pp \to A \to ZH$ with $H \to t\bar{t}$ (see Fig. 1), focusing on the mass range where one top quark is on-shell while the other is virtual. For this, we recast the ATLAS and CMS analyses of SM $t\bar{t}Z$ production [35, 36], which provide powerful experimental handles for such signatures [37].

From a theoretical perspective, the mass splitting among the components of an $SU(2)_L$ multiplet is governed by the electroweak (EW) vacuum expectation value (VEV) v: $m_A^2 = m_H^2 + \mathcal{O}(v^2)$. Consequently, for masses near the EW scale a gap exceeding the Z boson mass arises naturally while being consistent with perturbative unitarity, whereas for higher masses, such splittings are increasingly disfavored. This behavior is illustrated in Fig. 2, which shows the regions allowed by EW precision data and perturbative unitarity for different upper limits on the tree-level scattering amplitude. While a sizable part of the ATLAS search region does not satisfy these constraints, the low-mass region explored in this Letter

^{*} saiyad.ashanujjaman@kit.edu

 $^{^{\}dagger}$ guglielmo.coloretti@protonmail.com

[‡] andreas.crivellin@cern.ch

[§] siddharth.prasad.maharathy@cern.ch

[¶] bmellado@mail.cern.ch

 $^{^1}$ ATLAS considers $m_H > 350 \,\mathrm{GeV}$ and CMS $m_H > 330 \,\mathrm{GeV}$. Since CMS does not mention a $t\bar{t}$ threshold, it seems that they used the $\overline{\mathrm{MS}}$ mass for the top quark, whereas for the decay width the on-shell mass would be more appropriate. We therefore show the ATLAS search region in our plots.

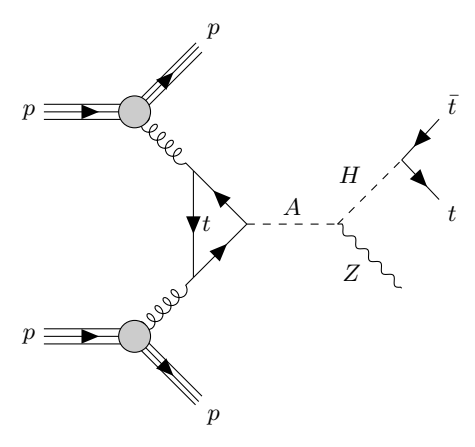


FIG. 1. Feynman diagram depicting the process $pp \to A \to ZH$ with $H \to t\bar{t}$, leading to a $t\bar{t}Z$ -like signature.

is fully populated by viable points in parameter space.

II. ANALYSES OF $t\bar{t}Z$ DIFFERENTIAL DISTRIBUTIONS

We consider a CP-odd Higgs boson A produced via gluon fusion at the LHC with the subsequent decays $A \to ZH$ and $H \to t\bar{t}$, where one of the top quarks is off-shell. The resulting $t\bar{t}Z$ -like signature enables us to exploit the measurements of the differential $t\bar{t}Z$ (and tWZ) cross sections by CMS [36] and ATLAS [35] to constrain this beyond-the-SM scenario.

The analysis targets final states with three or four leptons and at least one b-tagged jet, corresponding to $t\bar{t}Z$ (and tWZ) production in the SM. The CMS analysis provides results unfolded to the parton level (after radiation but before hadronization) and presents differential cross sections for five kinematic observables: the Z boson transverse momentum $(p_T(Z))$, the transverse momentum of the lepton from the W boson $(p_T(\ell_W))$, the azimuthal angle between the two Z leptons $(\Delta \phi(\ell^+, \ell^-))$, the angular separation between the Z boson and the Wboson lepton $(\Delta R(Z, \ell_W))$, and the cosine of the angle between the Z boson and the negatively charged lepton from its decay ($\cos \theta_Z^*$). The ATLAS analysis reports only $t\bar{t}Z$ differential cross sections, applying a more stringent requirement on the invariant mass of the opposite-sign lepton pair, unfolded to both particle and parton levels, covering 15 observables listed in Table 15 of Ref. [35].

To validate our setup, we simulate the SM processes $pp \to t\bar{t}Z$ and tWZ using MadGraph5_aMC_v3.5.3 [38, 39] with the NNPDF31_nlo_as_0118_1000 parton distribution function [40] at next-to-leading order (NLO) in QCD.² The obtained parton-level events are interfaced

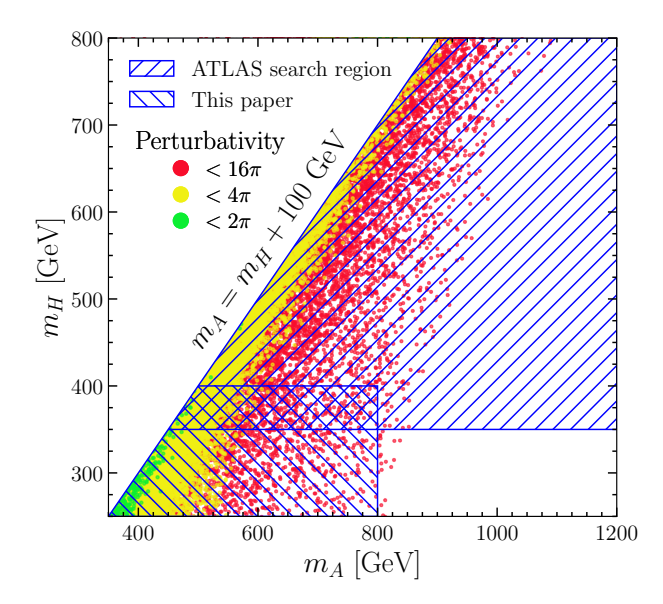


FIG. 2. Points allowed by EW precision data and perturbative unitarity for different upper limits on the tree-level scattering amplitudes: $<16\pi$ (red), $<4\pi$ (yellow) and $<2\pi$ (green). The search region from ATLAS, as well as the one covered in this work, is hatched. One can see that while only part of the ATLAS region contains viable points, our region is fully populated and closes the gap for $A\to ZH$ with $H\to t\bar t$ searches.

with Pythia 8.3 [42] using the CMS-CUETP8S1-CTEQ6L1 tune [43] to simulate particle decays, parton showering, and radiation. 3

For the reconstruction and selection of the leptons (electrons and muons) and jets (including b-tagged jets), we closely follow the CMS and ATLAS analyses; jets are clustered with the anti- k_T algorithm [44] implemented in FastJet 3.3.4 [45]. Events are required to contain at least three leptons, including a same-flavor opposite-sign pair with an invariant mass in the nominal Z boson window, and a third lepton consistent with a W boson decay. All additional selection requirements—jet and b-tagged jet multiplicities and kinematic thresholds on leptons and jets—are applied to reproduce the event selections used in the CMS and ATLAS signal regions.

We then simulate our new physics (NP) signal $pp \to A \to ZH$ with $H \to t\bar{t}$ using the same setup. To have an on-shell Z boson, we require a mass splitting $m_A - m_H \ge 100 \, \text{GeV}$. Our scan covers m_H from 260 GeV to 400 GeV (such that one top quark and the W boson originating from the off-shell top quark are on-shell) and m_A from 360 GeV to 800 GeV. The resulting differential distributions for the benchmark point $(m_A, m_H) = 0$

² At NLO, tWZ production interferes with the leading order ttZ process. To take this into account, we use the MadSTR plugin [41],

which removes overlap at the amplitude level using the diagram removal approach.

³ We previously applied the same strategy to constrain the WZ decay mode of a charged Higgs produced from top decays [37].

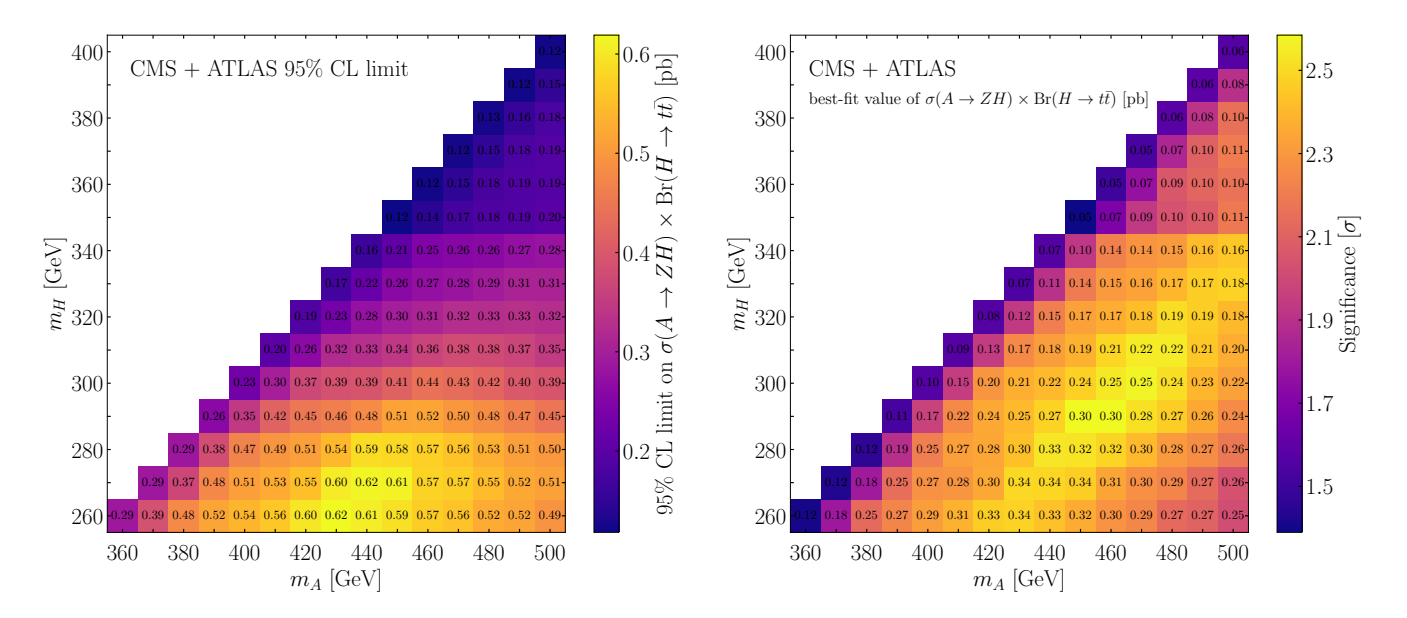


FIG. 3. 95% CL upper limit (left) and best-fit (right) value of $\sigma(A \to ZH) \times \text{Br}(H \to t\bar{t})$ in units of pb in the m_A - m_H plane with $m_A - m_H \ge 100 \,\text{GeV}$, obtained by combining the CMS and ATLAS analyses. The color bar in the left (right) plot indicates the 95% CL upper limit for the cross section (the preference for a non-zero NP signal in units of standard deviation). An extended region with $m_A < 800 \,\text{GeV}$ is provided in Fig. 9 in the Appendix.

(450, 290) GeV and $\sigma(A \to ZH) \times \text{Br}(H \to t\bar{t}) = 0.3 \text{ pb}$ are shown in the Appendix (Fig. 6 and Fig. 7).

III. RESULTS AND INTERPRETATION

The statistical model for the analysis is built from the binned data templates, SM predictions, and the NP contribution. The NP signal strength is extracted through a simultaneous χ^2 fit:

$$\chi^2 = [\sigma_i^{\rm data} - \sigma_i^{\rm theory}] \; \Sigma_{ij}^{-1} \; [\sigma_j^{\rm data} - \sigma_j^{\rm theory}] \; , \label{eq:chi_data}$$

where i, j run over the bins across all observables, Σ_{ij} denotes the covariance matrix, σ_i^{data} is the measured cross section in bin i, and

$$\sigma_i^{\text{theory}} = \mu_{\text{SM}} \, \sigma_i^{\text{SM}} + \mu_{\text{NP}} \, \sigma_i^{\text{NP}},$$

represents the expected cross section in bin i, with SM and NP contributions weighted by the corresponding fit parameters; $\mu_{\rm NP}$ is identified with $\sigma(A \to ZH) \times {\rm Br}(H \to t\bar{t})$. Correlations among the differential observables are obtained from our SM simulation, following Ref. [46].

For the CMS analysis, the theoretical uncertainties are given and incorporated by adding them in quadrature with the experimental ones, allowing us to fix $\mu_{\rm SM}=1.$ In contrast, the ATLAS measurement does not include or provide theoretical uncertainties. We thus use the MG5_aMC@NLO + Pythia 8 SM prediction, which lies in between the two simulations obtained from SHERPA (without and with multi-leg merging of additional partons) and take into account the theory error by profiling over

 $\mu_{\rm SM}$ by allowing a 5% deviation from 1, which corresponds approximately to the known uncertainty of the inclusive $t\bar{t}$ production cross section [47].

Using the global χ^2 (the sum of ATLAS and CMS), we extract model-independent limits on $\sigma(A \to ZH) \times$ $Br(H \to t\bar{t})$ in the m_A - m_H plane at 95% confidence level (CL). The resulting exclusion is shown in the left panel of Fig. 3. Furthermore, as illustrated in the right panel, the fit exhibits a mild (up to 2.5σ) preference for a non-zero NP signal, most pronounced around for $m_A \approx 450\text{--}460\,\text{GeV}$ and $m_H \approx 290\,\text{GeV}$, with a bestfit value of $\sigma(A \to ZH) \times \text{Br}(H \to t\bar{t}) \approx 0.3 \,\text{pb}$. Our limits are in good agreement with the dedicated ATLAS search for $A \to ZH$ with $H \to t\bar{t}$ in the overlap region, which demonstrates that reinterpretations of $t\bar{t}Z$ data can provide competitive sensitivity to heavy-Higgs signatures. For instance, at $m_A = 450(500) \,\text{GeV}$ and $m_H = 350(400)\,\mathrm{GeV}$, ATLAS reports a 95% CL limit of $\sigma(A \to ZH) \times \text{Br}(H \to t\bar{t}) \approx 0.13(0.14)$ pb in the narrow-width approximation [33], while our combined fit yields ≈ 0.12 pb, consistent with the expected improvement from including the CMS data.

A. Interpretation

We now interpret these results in the context of two-Higgs-doublet models (2HDM), focusing on the Type-I version and a top-philic scenario.

The Type I 2HDM [50] is a minimal extension of the SM obtained by introducing a second Higgs $SU(2)_L$ doublet, denoted Φ_1 [51], which does not couple to fermions, contrary to the SM-like Higgs doublet Φ_2 . In addition to

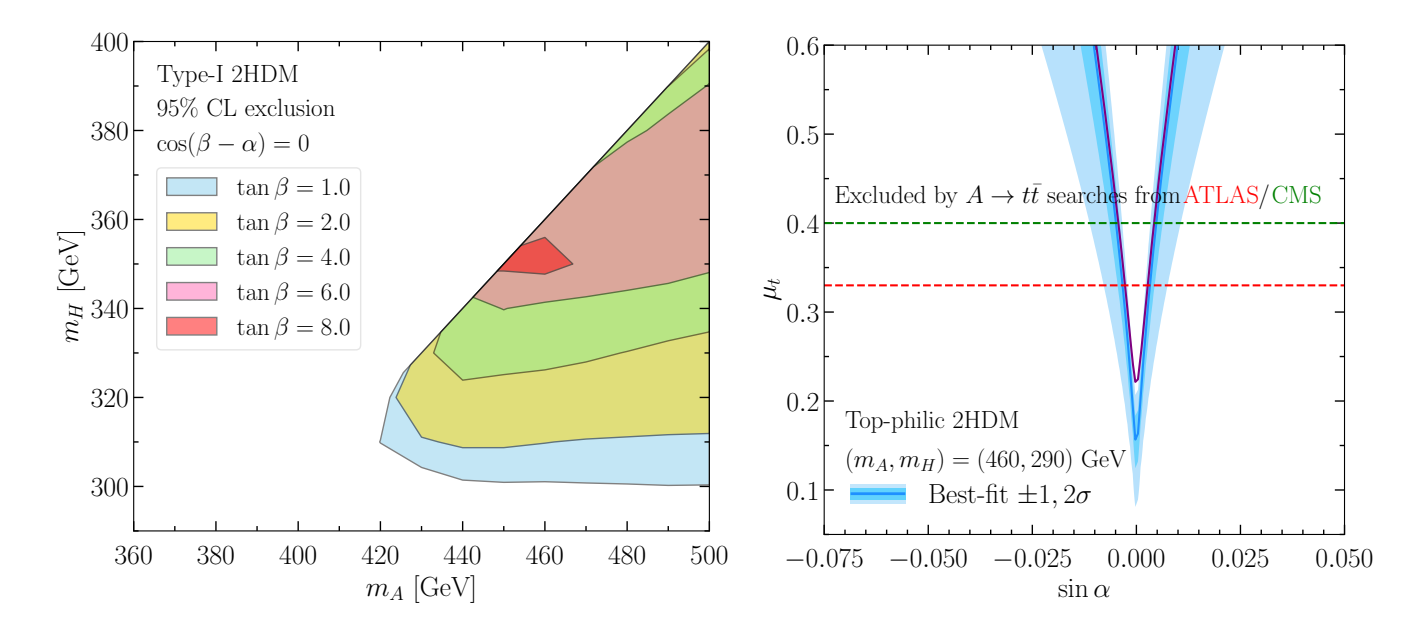


FIG. 4. Left: Regions in the m_A - m_H plane for the type-I 2HDM, assuming $\cos(\alpha - \beta) = 0$, that are excluded by our $A \to ZH$ with $H \to t\bar{t}$ analysis for different values of $\tan\beta$. Right: Preferred 1σ and 2σ region within the top-philic 2HDM for the best-fit point $m_A = 460\,\text{GeV}$ and $m_H = 290\,\text{GeV}$ where a 2.5σ preference is observed. The purple curve denotes the best-fit for the aligned 2HDM with $\xi_u \neq 0$. The regions above the red and green lines are excluded by the ATLAS and CMS searches for $A \to t\bar{t}$ [48, 49], respectively.

the Higgs masses— $m_h=125\,\mathrm{GeV},\ m_H\ (CP\text{-}\mathrm{even}),\ m_A\ (CP\text{-}\mathrm{odd})$ and m_{H^\pm} (charged)—the scalar sector is characterized by the ratio of the two VEVs ($\tan\beta=v_2/v_1$), the mixing angle between the CP-even Higgs states (α), and the quartic coupling λ_5 associated with the term $(\Phi_1^{\dagger}\Phi_2)^2$. The decoupling limit is achieved for $\alpha\to 0$ and m_A, m_H, m_{H^\pm} and $\tan\beta\to\infty$.

Assuming $m_A < m_{H^{\pm}} + m_W$, such that the decay $A \to H^{\pm}W$ is not possible, the branching ratio of $A \to ZH$ is controlled by m_A , m_H and the couplings $g_{AZH} \propto \sin(\beta - \alpha)$ and $y_A^f \propto \cot \beta$. Br $(A \to ZH)$ therefore increases with $\tan \beta$, due to the suppression of fermionic decays, and grows with $m_A - m_H$. The subsequent decay of H is governed by its couplings to fermions and gauge bosons, $y_H^f \propto \sin \alpha / \sin \beta$ and $g_{HVV} \propto \cos(\beta - \alpha)$. Thus, the $H \to t\bar{t}$ mode dominates close to the alignment limit $\sin(\beta - \alpha) \approx 1$.

We show in the left panel of Fig. 4 the excluded regions in the m_A – m_H plane for different values of $\tan \beta$. Note that most of this parameter space was previously not covered by dedicated $A \to ZH$ searches and allowed by Higgs signal strength measurements, electroweak precision data, perturbative unitarity, and vacuum stability (see Fig. 8 in the Appendix for details). Furthermore, for $\tan \beta \gtrsim 2$, the bounds from $A, H \to t\bar{t}$ [48, 49] and $tb(H^\pm \to tb)$ [52, 53] are generally satisfied. Therefore, the limits we derive here provide the most stringent constraints in the considered regions of the type-I 2HDM parameter space.

For the best fit point for the masses $m_A \simeq 450 \,\text{GeV} - 460 \,\text{GeV}$ and $m_H \simeq 290 \,\text{GeV}$ (see right plot in Fig. 3),

we do not obtain relevant constraints in Type-I 2HDM (see the left plot in Fig. 3), since only very small values of $\tan \beta$ can account for the upper limit on the signal strength. Consequently, accommodating the observed preference for a non-zero NP contribution within the Type-I 2HDM is challenging, we turn to the top-philic 2HDM. This simplified model can be realized within the 2HDM with generic Yukawa couplings (Type III) [54, 55] by working in the Higgs basis (where only one doublet acquires a vacuum expectation value [56]) and assuming that the other doublet couples exclusively to the top quark. Normalizing the Yukawa interaction of the second doublet to the SM top Yukawa, $\mu_t Y_t \bar{Q}_3 \Phi_1 u_3$, we find that the preference for a non-vanishing NP contribution at $m_A \simeq 450\text{--}460~\mathrm{GeV}$ and $m_H \simeq 290~\mathrm{GeV}$ can be explained for $\mu_t \gtrsim 0.16$ and $\sin \alpha \sim 0$; see Fig. 4 (right). The 1σ and 2σ regions (shaded in blue) and the regions excluded by the CMS and ATLAS searches for $A \to t\bar{t}$ [48, 49] are shown. In addition, since the top-philic 2HDM can be approximately realized in the aligned 2HDM [57] by assuming that only ξ_u differs from zero (with $\xi_d = \xi_\ell = 0$), we also show the best fit line (purple) for this model.

IV. CONCLUSIONS AND OUTLOOK

In this article, we derived novel limits on the cross section of the process $pp \to A \to ZH$ with $H \to t\bar{t}$ in the low-mass region where one of the top quarks is offshell. This part of parameter space was previously not

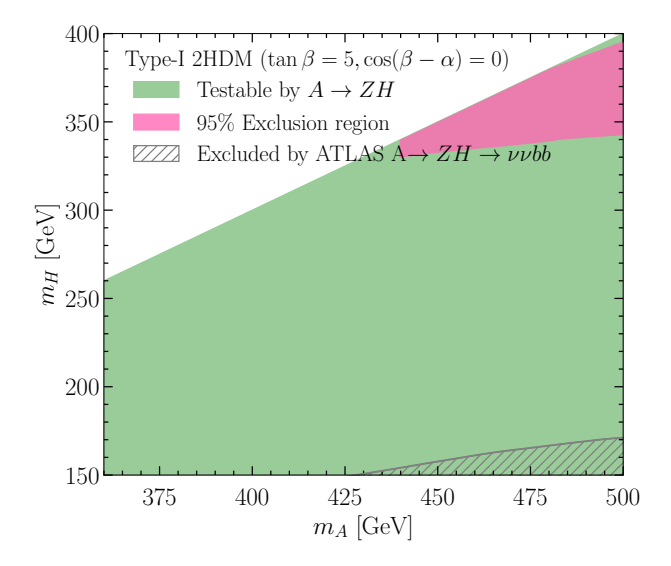


FIG. 5. Regions in the m_A-m_H plane with $m_A-m_H \geq 100$ GeV for the Type I 2HDM, assuming $\cos(\alpha-\beta)=0$ and $\tan\beta=5$. The green area denotes the parameter space consistent with theoretical constraints, the SM Higgs diphoton rate [58], electroweak precision observables [59], and limits on the charged Higgs mass from $B\to X_s\gamma$ [60]. The pink area is excluded by our analysis, while the black hatched region is ruled out by the ATLAS $A\to ZH\to \nu\nu\nu b\bar{b}$ search [48].

explored by dedicated ATLAS and CMS analyses, despite being well motivated: a sizable mass splitting between the neutral Higgs states is more naturally realized near the EW scale than for higher masses, i.e., the consistency with perturbative unitarity is better (see Fig. 2).

We obtained limits on $\sigma(A \to ZH) \times \text{Br}(H \to t\bar{t})$ in the range 0.12–0.62 pb for $m_A > m_H + 100\,\text{GeV}$ and m_A between 360 GeV and 500 GeV, which are in good agreement with the dedicated ATLAS and CMS searches in the overlapping mass region. These strong bounds are obtained despite a preference (up to $\sim 2.5\sigma$) for an NP signal around $m_A \simeq 450\,\text{GeV}$ –460 GeV and $m_H \simeq 290\,\text{GeV}$.

Interpreting the results within the Type-I 2HDM, we find that a sizable part of the m_A – m_H plane can be excluded for $\tan \beta \lesssim 8$, a region that was previously unconstrained; see Fig. 4 (left) and Fig. 5. Finally, the observed preference for a non-zero NP signal can be accommodated in the top-philic 2HDM for $\mu_t \gtrsim 0.16$. Future high-luminosity LHC measurements of differential $t\bar{t}Z$ production and dedicated searches for $A \to ZH$ with $H \to t\bar{t}$ will allow this region to be probed with greater precision and result in an enlarged exclusion region in Fig. 5 (or a potential NP discovery), providing a direct test of the top-philic Higgs scenario like the aligned 2HDM with $\xi_{d,\ell} \approx 0$ but $\xi_u \neq 0$. In general, our analysis shows the importance and feasibility of searching for Higgs signals with off-shell top quarks in the final state.

ACKNOWLEDGMENTS

SA is supported by the Deutsche Forschungsgemeinschaft (DFG, German Research Foundation) under grant 396021762 – TRR 257. AC is supported by a professorship grant of the Swiss National Science Foundation (Grant No. PP00P21_76884). SPM and BM acknowledge the support of the Research Office of the University of the Witwatersrand. BM further acknowledges support from the South African Department of Science and Innovation through the SA-CERN program, and the National Research Foundation.

Appendix

The differential cross sections for the observables measured by CMS and ATLAS are shown in Fig. 6 and Fig. 7, respectively. The data and the SM predictions are taken from each analysis, while the NP predictions correspond to $(m_A, m_H) = (460, 290) \, \text{GeV}$ for the (combined) best-fit point $\sigma(A \to ZH) \times \text{Br}(H \to t\bar{t}) \approx 0.3 \, \text{pb}$.

In Fig. 8, we present the parameter space of the Type-I 2HDM that is consistent with theoretical and experimental constraints, including perturbative unitarity, vacuum stability, the SM Higgs di-photon signal strength [58], electroweak precision observables [59], and bounds on the charged Higgs mass from inclusive weak radiative B-meson decays [60]. The shown range corresponds to the parameter region explored in our analysis.

Finally, Fig. 9 displays the extended m_A – m_H plane with the resulting 95% CL upper limits on $\sigma(A \to ZH) \times Br(H \to t\bar{t})$, extending the results of Fig. 3.

REFERENCES

- P. W. Higgs, Broken symmetries, massless particles and gauge fields, Phys. Lett. 12, 132 (1964).
- [2] F. Englert and R. Brout, Broken Symmetry and the Mass of Gauge Vector Mesons, Phys. Rev. Lett. 13, 321 (1964).
- [3] P. W. Higgs, Broken Symmetries and the Masses of Gauge Bosons, Phys. Rev. Lett. 13, 508 (1964).
- [4] G. S. Guralnik, C. R. Hagen, and T. W. B. Kibble, Global Conservation Laws and Massless Particles, Phys. Rev. Lett. 13, 585 (1964).
- [5] G. Aad et al. (ATLAS), Observation of a new particle in the search for the Standard Model Higgs boson with the ATLAS detector at the LHC, Phys. Lett. B 716, 1 (2012), arXiv:1207.7214 [hep-ex].
- [6] S. Chatrchyan et al. (CMS), Observation of a New Boson at a Mass of 125 GeV with the CMS Experiment at the LHC, Phys. Lett. B 716, 30 (2012), arXiv:1207.7235 [hep-ex].
- [7] J. M. Langford (ATLAS, CMS), Combination of Higgs measurements from ATLAS and CMS: couplings and ||framework, PoS LHCP2020, 136 (2021).
- [8] Combined measurements of Higgs boson production and decay using up to $139~{\rm fb}^{-1}$ of proton-proton collision data

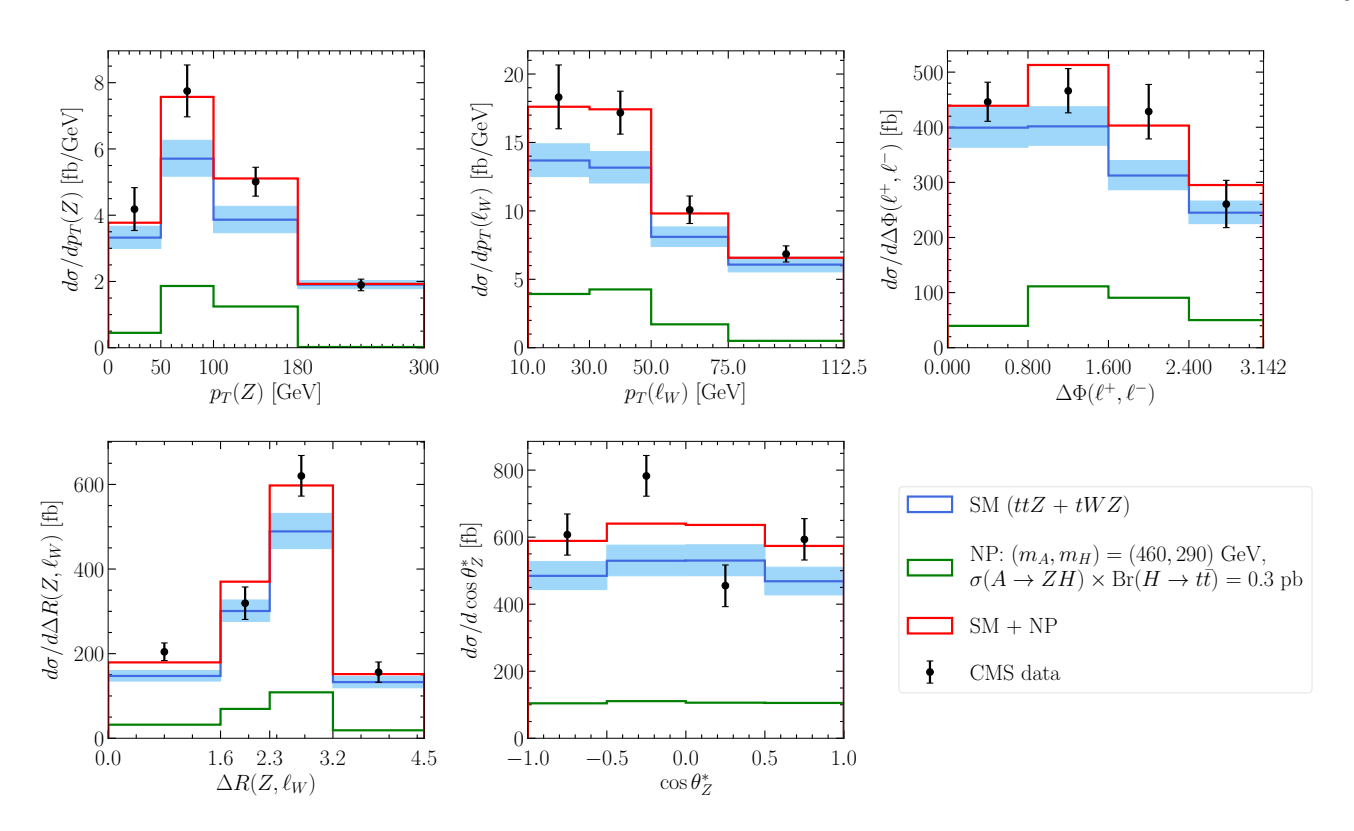


FIG. 6. $t\bar{t}Z + tWZ$ differential cross sections for various observables measured by CMS. The error bars indicate the total experimental error, while the shaded blue area corresponds to the theory uncertainty. The NP contributions are shown for $(m_A, m_H) = (460, 290) \,\text{GeV}$ and $\sigma(A \to ZH) \times \text{Br}(H \to t\bar{t}) = 0.3 \,\text{pb}$, corresponding to the combined (ATLAS and CMS) best-fit point.

- at $\sqrt{s} = 13$ TeV collected with the ATLAS experiment, (2021).
- [9] V. Silveira and A. Zee, SCALAR PHANTOMS, Phys. Lett. B 161, 136 (1985).
- [10] M. Pietroni, The Electroweak phase transition in a nonminimal supersymmetric model, Nucl. Phys. B 402, 27 (1993), arXiv:hep-ph/9207227.
- [11] J. McDonald, Gauge singlet scalars as cold dark matter, Phys. Rev. D 50, 3637 (1994), arXiv:hep-ph/0702143.
- [12] T. D. Lee, A Theory of Spontaneous T Violation, Phys. Rev. D 8, 1226 (1973).
- [13] P. Fayet, Supergauge Invariant Extension of the Higgs Mechanism and a Model for the electron and Its Neutrino, Nucl. Phys. B 90, 104 (1975).
- [14] P. Fayet, Spontaneously Broken Supersymmetric Theories of Weak, Electromagnetic and Strong Interactions, Phys. Lett. B 69, 489 (1977).
- [15] H. E. Haber and G. L. Kane, The Search for Supersymmetry: Probing Physics Beyond the Standard Model, Phys. Rept. 117, 75 (1985).
- [16] J. E. Kim, Light Pseudoscalars, Particle Physics and Cosmology, Phys. Rept. 150, 1 (1987).
- [17] R. D. Peccei and H. R. Quinn, CP Conservation in the Presence of Instantons, Phys. Rev. Lett. 38, 1440 (1977).
- [18] N. Turok and J. Zadrozny, Electroweak baryogenesis in the two doublet model, Nucl. Phys. B 358, 471 (1991).
- [19] D. A. Ross and M. J. G. Veltman, Neutral currents and the Higgs mechanism, Nucl. Phys. B 95, 135 (1975).
- [20] W. Konetschny and W. Kummer, Nonconservation of To-

- tal Lepton Number with Scalar Bosons, Phys. Lett. B 70, 433 (1977).
- [21] T. P. Cheng and L.-F. Li, Neutrino Masses, Mixings and Oscillations in SU(2) x U(1) Models of Electroweak Interactions, Phys. Rev. D 22, 2860 (1980).
- [22] G. Lazarides, Q. Shafi, and C. Wetterich, Proton Lifetime and Fermion Masses in an SO(10) Model, Nucl. Phys. B 181, 287 (1981).
- [23] J. Schechter and J. W. F. Valle, Neutrino Masses in SU(2) x U(1) Theories, Phys. Rev. D 22, 2227 (1980).
- [24] M. Magg and C. Wetterich, Neutrino Mass Problem and Gauge Hierarchy, Phys. Lett. B 94, 61 (1980).
- [25] R. N. Mohapatra and G. Senjanovic, Neutrino Masses and Mixings in Gauge Models with Spontaneous Parity Violation, Phys. Rev. D 23, 165 (1981).
- [26] J. F. Gunion, R. Vega, and J. Wudka, Higgs triplets in the standard model, Phys. Rev. D 42, 1673 (1990).
- [27] T. G. Rizzo, Updated bounds on Higgs triplet vacuum expectation values and the tree level rho parameter from radiative corrections, Mod. Phys. Lett. A 6, 1961 (1991).
- [28] P. Chardonnet, P. Fayet, and P. Salati, Heavy triplet neutrinos as a new dark matter option, Nucl. Phys. B 394, 35 (1993).
- [29] T. Blank and W. Hollik, Precision observables in SU(2) x U(1) models with an additional Higgs triplet, Nucl. Phys. B 514, 113 (1998), arXiv:hep-ph/9703392.
- [30] G. Aad et al. (ATLAS), ATLAS searches for additional scalars and exotic Higgs boson decays with the LHC Run 2 dataset, Phys. Rept. 1116, 184 (2025),

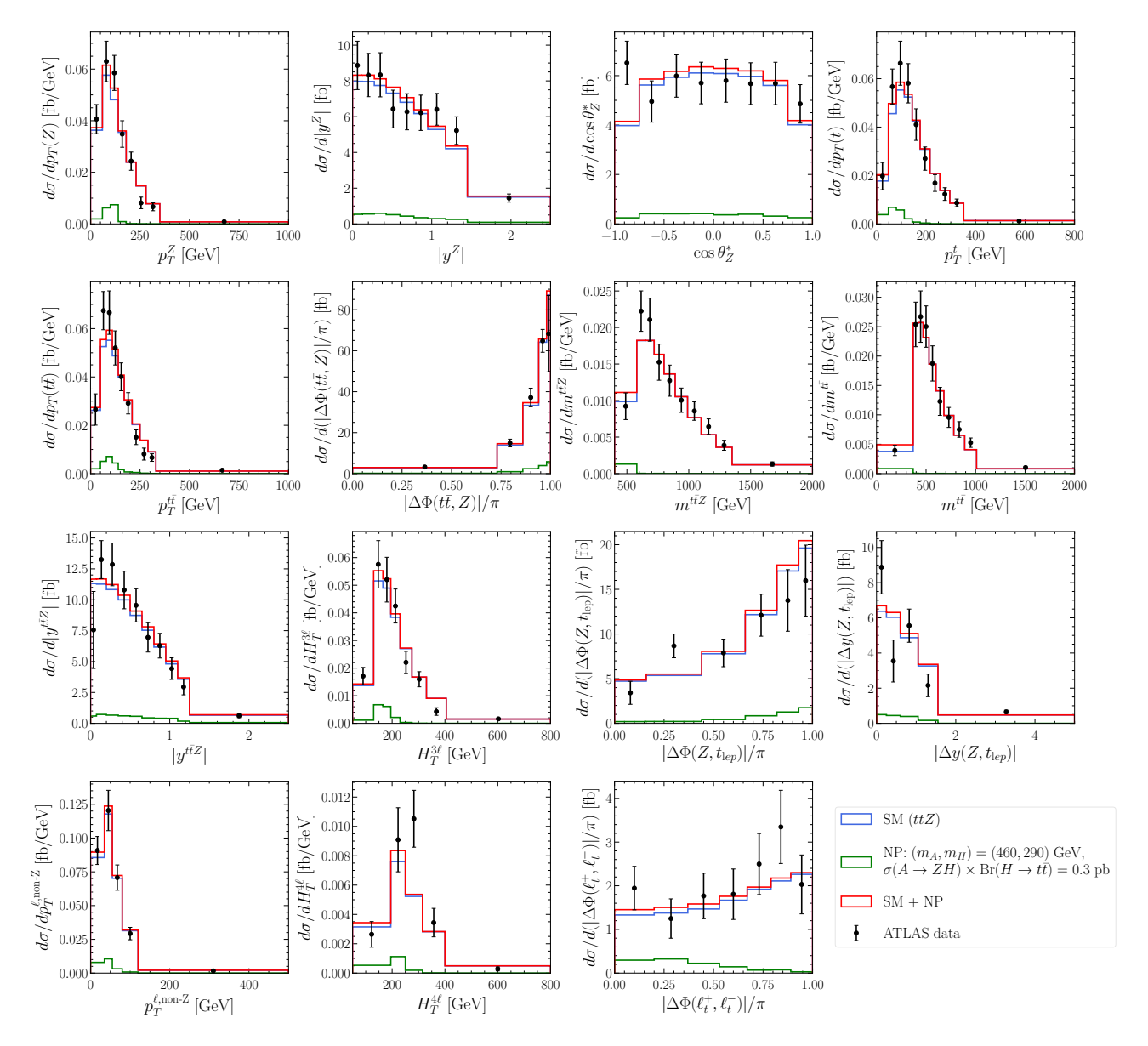


FIG. 7. Differential $t\bar{t}Z$ cross sections unfolded to particle level for different observables measured by ATLAS. The error bars indicate the total experimental uncertainties. The NP contributions are shown for $(m_A, m_H) = (460, 290) \,\text{GeV}$ and $\sigma(A \to ZH) \times \text{Br}(H \to t\bar{t}) = 0.3 \,\text{pb}$, corresponding to the combined (ATLAS and CMS) best-fit point.

arXiv:2405.04914 [hep-ex].

- [31] A. Hayrapetyan et al. (CMS), Searches for Higgs boson production through decays of heavy resonances, Phys. Rept. 1115, 368 (2025), arXiv:2403.16926 [hep-ex].
- [32] G. C. Dorsch, S. J. Huber, K. Mimasu, and J. M. No, Echoes of the Electroweak Phase Transition: Discovering a second Higgs doublet through $A_0 \to ZH_0$, Phys. Rev. Lett. **113**, 211802 (2014), arXiv:1405.5537 [hep-ph].
- [33] G. Aad *et al.* (ATLAS), Search for a CP-odd Higgs boson decaying into a heavy CP-even Higgs boson and a Z boson in the $\ell^+\ell^-t\bar{t}$ and $\nu\bar{\nu}b\bar{b}$ final states using 140 fb⁻¹ of data collected with the ATLAS detector, JHEP **02**, 197, arXiv:2311.04033 [hep-ex].
- [34] A. Hayrapetyan et al. (CMS), Search for heavy neutral Higgs bosons A and H in the $t\bar{t}Z$ channel in proton-

- proton collisions at 13 TeV, Phys. Lett. B **866**, 139568 (2025), arXiv:2412.00570 [hep-ex].
- [35] G. Aad et al. (ATLAS), Inclusive and differential cross-section measurements of $t\bar{t}Z$ production in pp collisions at $\sqrt{s}=13$ TeV with the ATLAS detector, including EFT and spin-correlation interpretations, JHEP 07, 163, arXiv:2312.04450 [hep-ex].
- [36] A. Hayrapetyan *et al.* (CMS), Measurements of inclusive and differential cross sections for top quark production in association with a Z boson in proton-proton collisions at $\sqrt{s} = 13 \text{ TeV}$, JHEP **02**, 177, arXiv:2410.23475 [hep-ex].
- [37] S. Ashanujjaman, A. Crivellin, S. P. Maharathy, and B. Mellado, Searching for a Charged Higgs Boson in Top-Quark Decays via the WZ Mode, (2025), arXiv:2509.07094 [hep-ph].

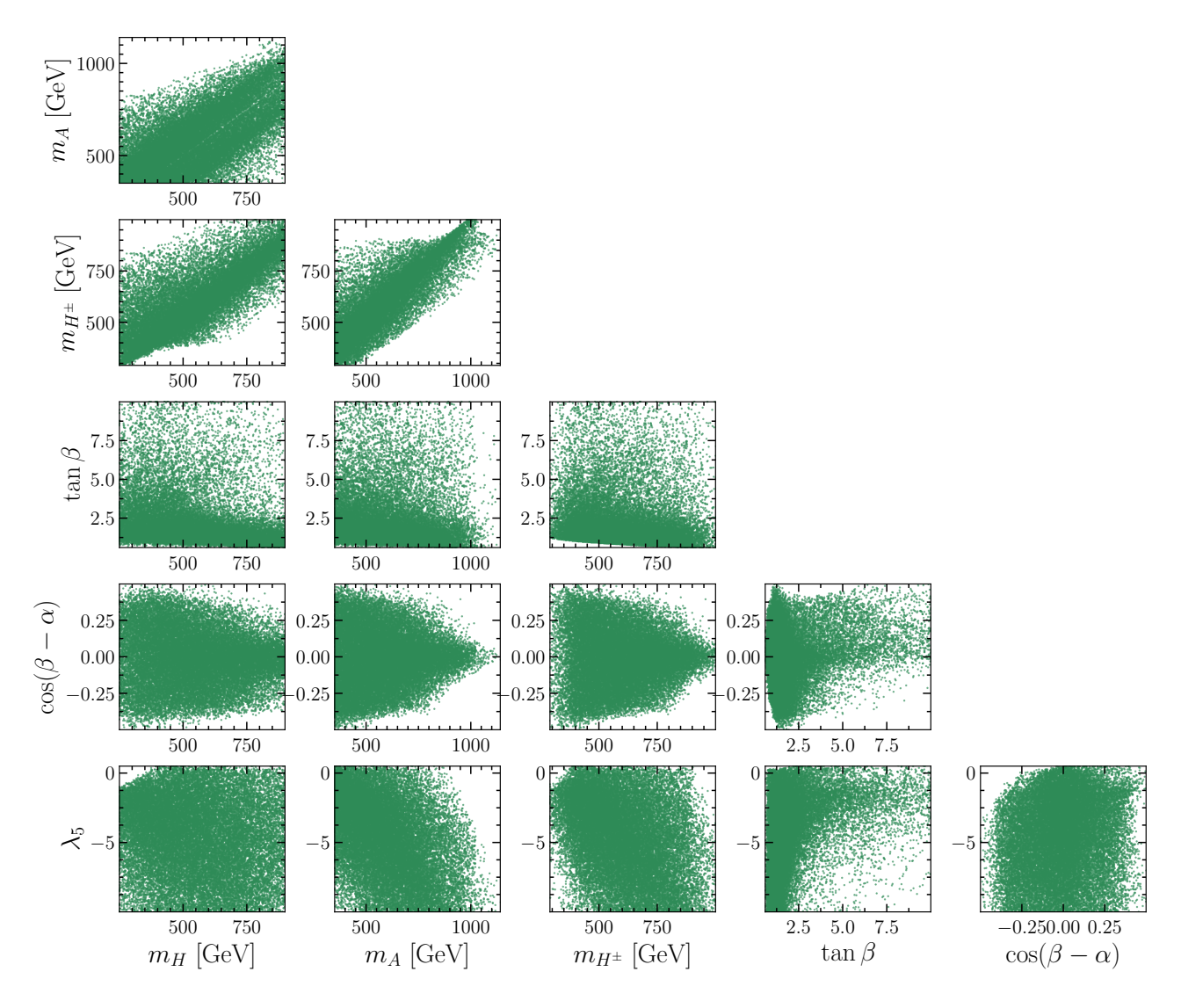


FIG. 8. Parameter space of the type-I 2HDM allowed by theoretical constraints (perturbative unitarity and vacuum stability), the SM Higgs di-photon signal strength [58], electroweak precision data [59], and bounds on the charged Higgs mass from inclusive weak radiative *B*-meson decays [60]. The plot range also corresponds to the scan range.

- [38] J. Alwall, R. Frederix, S. Frixione, V. Hirschi, F. Maltoni, O. Mattelaer, H. S. Shao, T. Stelzer, P. Torrielli, and M. Zaro, The automated computation of tree-level and next-to-leading order differential cross sections, and their matching to parton shower simulations, JHEP 07, 079, arXiv:1405.0301 [hep-ph].
- [39] R. Frederix, S. Frixione, V. Hirschi, D. Pagani, H. S. Shao, and M. Zaro, The automation of next-to-leading order electroweak calculations, JHEP 07, 185, [Erratum: JHEP 11, 085 (2021)], arXiv:1804.10017 [hep-ph].
- [40] R. D. Ball et al. (NNPDF), Parton distributions from high-precision collider data, Eur. Phys. J. C 77, 663 (2017), arXiv:1706.00428 [hep-ph].
- [41] S. Frixione, B. Fuks, V. Hirschi, K. Mawatari, H.-S. Shao, P. A. Sunder, and M. Zaro, Automated simulations beyond the Standard Model: supersymmetry, JHEP 12, 008, arXiv:1907.04898 [hep-ph].
- [42] T. Sjöstrand, S. Ask, J. R. Christiansen, R. Corke, N. Desai, P. Ilten, S. Mrenna, S. Prestel, C. O. Rasmussen, and

- P. Z. Skands, An introduction to PYTHIA 8.2, Comput. Phys. Commun. **191**, 159 (2015), arXiv:1410.3012 [hep-ph].
- [43] V. Khachatryan et al. (CMS), Event generator tunes obtained from underlying event and multiparton scattering measurements, Eur. Phys. J. C 76, 155 (2016), arXiv:1512.00815 [hep-ex].
- [44] M. Cacciari, G. P. Salam, and G. Soyez, The anti- k_t jet clustering algorithm, JHEP **04**, 063, arXiv:0802.1189 [hep-ph].
- [45] M. Cacciari, G. P. Salam, and G. Soyez, FastJet User Manual, Eur. Phys. J. C 72, 1896 (2012), arXiv:1111.6097 [hep-ph].
- [46] S. Banik, G. Coloretti, A. Crivellin, and B. Mellado, Uncovering new Higgses in the LHC analyses of differential tt̄ cross sections, JHEP 01, 155, arXiv:2308.07953 [hep-ph].
- [47] M. Czakon and A. Mitov, Top++: A Program for the Calculation of the Top-Pair Cross-Section at Hadron

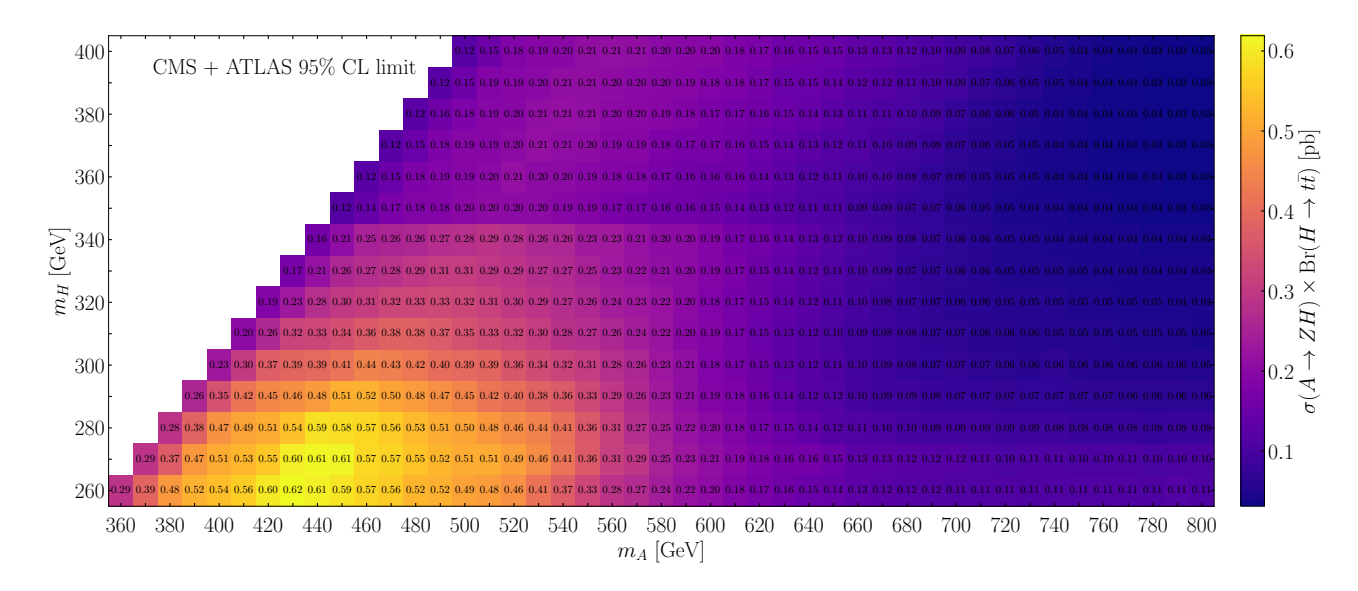


FIG. 9. Extended 95% CL upper limits on $\sigma(A \to ZH) \times \text{Br}(H \to t\bar{t})$ in units of pb in the m_A - m_H plane with $m_A - m_H \ge 100$ GeV. This plot extends the results shown in Fig. 3 to a wider mass range.

Colliders, Comput. Phys. Commun. **185**, 2930 (2014), arXiv:1112.5675 [hep-ph].

- [48] G. Aad *et al.* (ATLAS), Search for heavy neutral Higgs bosons decaying into a top quark pair in 140 fb⁻¹ of proton-proton collision data at $\sqrt{s} = 13$ TeV with the ATLAS detector, JHEP 08, 013, arXiv:2404.18986 [hepex].
- [49] A. Hayrapetyan *et al.* (CMS), Search for heavy pseudoscalar and scalar bosons decaying to a top quark pair in proton-proton collisions at $\sqrt{s} = 13$ TeV, (2025), arXiv:2507.05119 [hep-ex].
- [50] S. L. Glashow and S. Weinberg, Natural Conservation Laws for Neutral Currents, Phys. Rev. D 15, 1958 (1977).
- [51] G. C. Branco, P. M. Ferreira, L. Lavoura, M. N. Rebelo, M. Sher, and J. P. Silva, Theory and phenomenology of two-Higgs-doublet models, Phys. Rept. 516, 1 (2012), arXiv:1106.0034 [hep-ph].
- [52] A. M. Sirunyan *et al.* (CMS), Search for a charged Higgs boson decaying into top and bottom quarks in events with electrons or muons in proton-proton collisions at $\sqrt{s} = 13$ TeV, JHEP **01**, 096, arXiv:1908.09206 [hep-ex].
- [53] G. Aad *et al.* (ATLAS), Search for charged Higgs bosons decaying into a top quark and a bottom quark at \sqrt{s} = 13 TeV with the ATLAS detector, JHEP **06**, 145, arXiv:2102.10076 [hep-ex].

- [54] D. Atwood, L. Reina, and A. Soni, Phenomenology of two Higgs doublet models with flavor changing neutral currents, Phys. Rev. D 55, 3156 (1997), arXiv:hepph/9609279.
- [55] A. Crivellin, A. Kokulu, and C. Greub, Flavor-phenomenology of two-Higgs-doublet models with generic Yukawa structure, Phys. Rev. D 87, 094031 (2013), arXiv:1303.5877 [hep-ph].
- [56] S. Davidson and H. E. Haber, Basis-independent methods for the two-Higgs-doublet model, Phys. Rev. D 72, 035004 (2005), [Erratum: Phys.Rev.D 72, 099902 (2005)], arXiv:hep-ph/0504050.
- [57] A. Pich and P. Tuzon, Yukawa Alignment in the Two-Higgs-Doublet Model, Phys. Rev. D 80, 091702 (2009), arXiv:0908.1554 [hep-ph].
- [58] Y. Heo, D.-W. Jung, and J. S. Lee, Higgs boson precision analysis of the full LHC run 1 and run 2 data, Phys. Rev. D 110, 013003 (2024), arXiv:2402.02822 [hep-ph].
- [59] S. Navas et al. (Particle Data Group), Review of particle physics, Phys. Rev. D 110, 030001 (2024).
- [60] M. Misiak and M. Steinhauser, Weak radiative decays of the B meson and bounds on M_{H^\pm} in the Two-Higgs-Doublet Model, Eur. Phys. J. C 77, 201 (2017), arXiv:1702.04571 [hep-ph].